AMERICAN SOCIETY FOR MICROBIOLOGY | mSphere®

RESEARCH ARTICLE
Molecular Biology and Physiology

# The Two-Component System CopRS Maintains Subfemtomolar Levels of Free Copper in the Periplasm of *Pseudomonas aeruginosa* Using a Phosphatase-Based Mechanism

**Lorena Novoa-Aponte,[a] Cheng Xu,[a] Fernando C. Soncini,[b] José M. Argüello[a]**

[a]Department of Chemistry and Biochemistry, Worcester Polytechnic Institute, Worcester, Massachusetts, USA
[b]Instituto de Biología Molecular y Celular de Rosario, Universidad Nacional de Rosario, Consejo Nacional de Investigaciones Científicas y Técnicas, Rosario, Santa Fe, Argentina

**ABSTRACT** Two-component systems control periplasmic $Cu^{+}$ homeostasis in Gram-negative bacteria. In characterized systems such as *Escherichia coli* CusRS, upon $Cu^{+}$ binding to the periplasmic sensing region of CusS, a cytoplasmic phosphotransfer domain of the sensor phosphorylates the response regulator CusR. This drives the expression of efflux transporters, chaperones, and redox enzymes to ameliorate metal toxic effects. Here, we show that the *Pseudomonas aeruginosa* two-component sensor histidine kinase CopS exhibits a Cu-dependent phosphatase activity that maintains CopR in a nonphosphorylated state when the periplasmic Cu levels are below the activation threshold of CopS. Upon $Cu^{+}$ binding to the sensor, the phosphatase activity is blocked and the phosphorylated CopR activates transcription of the CopRS regulon. Supporting the model, mutagenesis experiments revealed that the Δ*copS* strain exhibits maximal expression of the CopRS regulon, lower intracellular $Cu^{+}$ levels, and increased Cu tolerance compared to wild-type cells. The invariant phosphoacceptor residue $His_{235}$ of CopS was not required for the phosphatase activity itself but was necessary for its Cu dependency. To sense the metal, the periplasmic domain of CopS binds two $Cu^{+}$ ions at its dimeric interface. Homology modeling of CopS based on CusS structure (four $Ag^{+}$ binding sites) clearly supports the different binding stoichiometries in the two systems. Interestingly, CopS binds $Cu^{+/2+}$ with $3 \times 10^{-14}$ M affinity, pointing to the absence of free (hydrated) $Cu^{+/2+}$ in the periplasm.

**IMPORTANCE** Copper is a micronutrient required as cofactor in redox enzymes. When free, copper is toxic, mismetallating proteins and generating damaging free radicals. Consequently, copper overload is a strategy that eukaryotic cells use to combat pathogens. Bacteria have developed copper-sensing transcription factors to control copper homeostasis. The cell envelope is the first compartment that has to cope with copper stress. Dedicated two-component systems control the periplasmic response to metal overload. This paper shows that the sensor kinase of the copper-sensing two-component system present in *Pseudomonadales* exhibits a signal-dependent phosphatase activity controlling the activation of its cognate response regulator, distinct from previously described periplasmic Cu sensors. Importantly, the data show that the system is activated by copper levels compatible with the absence of free copper in the cell periplasm. These observations emphasize the diversity of molecular mechanisms that have evolved in bacteria to manage the copper cellular distribution.

**KEYWORDS** *Pseudomonas aeruginosa*, copper, homeostasis, periplasm, two-component regulatory systems

Copper is a cellular micronutrient required for redox enzymatic functions (1, 2). However, free Cu undergoes deleterious Fenton reactions, metallates noncognate binding sites, and promotes disassembly of Fe-S centers (3, 4). Early studies in the field

**Citation** Novoa-Aponte L, Xu C, Soncini FC, Argüello JM. 2020. The two-component system CopRS maintains subfemtomolar levels of free copper in the periplasm of *Pseudomonas aeruginosa* using a phosphatase-based mechanism. mSphere 5:e01193-20. https://doi.org/10.1128/mSphere.01193-20.

**Editor** Craig D. Ellermeier, University of Iowa



Address correspondence to José M. Argüello, arguello@wpi.edu.

**Received** 24 November 2020
**Accepted** 27 November 2020
**Published** 23 December 2020

took advantage of Cu toxicity to identify widely distributed proteins conferring metal tolerance, namely, metal-sensing transcriptional regulators and efflux transporters (1, 4–7). Recent studies have, however, started to uncover regulated distribution systems that move the metal among cellular compartments and target $Cu^+$ to cognate metalloproteins while maintaining the required homeostasis (8–15). These include $Cu^+$-sensing transcriptional regulators, influx and efflux transmembrane transporters, chaperones, and storage molecules. In this context, bacterial cells prevent Cu toxicity by expressing some of these molecules in response to high intracellular metal conditions. The cytoplasmic response to $Cu^+$ excess has been characterized in numerous Gram-positive and Gram-negative bacteria (11, 16–19). Nevertheless, periplasmic components involved in $Cu^+$ homeostasis have received much less attention. A simple consideration of the Gram-negative bacterium architecture points out that periplasmic dyshomeostasis is likely to precede the cytoplasmic response to a surge of $Cu^+$ influx. Supporting this idea, mathematical simulations based on $Cu^+$ uptake experiments in *Pseudomonas aeruginosa* under dyshomeostasis conditions suggest that the periplasmic $Cu^+$ overload precedes the cytoplasmic imbalance (10). Moreover, periplasmic storage molecules are likely crucial for maintaining cellular $Cu^+$ allocation (10).

Cytoplasmic $Cu^+$-sensing transcriptional regulators are diverse, as different bacterial species have solved $Cu^+$ homeostasis using alternative strategies (1, 5, 20, 21). However, the periplasmic response appears usually regulated by similar two-component systems (TCSs) (22, 23). Although absent in *Salmonella* (6), many *Enterobacteriaceae* (e.g., *Escherichia coli*, *Klebsiella pneumoniae*, etc.) modulate periplasmic $Cu^+$ stress responses via the chromosomally encoded TCS CusRS and the plasmid-borne PcoRS (24–30). Instead, CopRS monitors extracytoplasmic $Cu^+$ accumulation in *Corynebacterium glutamicum* and *Synechocystis* (31–33). CopRS is also found in *Pseudomonadaceae*, including *Pseudomonas syringae* (34, 35), *P. aeruginosa* (9), and *Pseudomonas fluorescens* (36, 37).

Most TCSs comprise a sensor histidine kinase (SHK) and its cognate cytoplasmic response regulator (RR). The SHK is usually a homodimeric membrane receptor with a periplasmic sensor domain flanked by two transmembrane segments (see Fig. S1 in the supplemental material). The C-terminal cytoplasmic domain contains the catalytic machinery (38). SHKs are bifunctional enzymes that switch between kinase and phosphatase states in a signal-dependent manner. In the kinase mode, the SHK undergoes autophosphorylation of a conserved His residue and subsequently transfers the phosphoryl group to a conserved Asp residue of its cognate RR. Although some RRs have alternative roles in their unphosphorylated states (39), phosphorylation of most of the RRs allosterically modifies their transcriptional activity (Fig. 1A). TCS sensors might also operate in a phosphatase mode. In these cases, the dephosphorylated SHK catalyzes the dephosphorylation of RR (RR∼P) that has been phosphorylated, metabolically or by an alternative kinase, in response to an environmental stimulus (39–43).

Ultimately, the signal-dependent balance between SHK kinase and phosphatase activities determines the RR∼P levels, modulating the output response (38). In the archetypical *E. coli* CusRS TCS, $Cu^+$ binding to the periplasmic loop of CusS promotes its autophosphorylation and the subsequent phosphorylation of the transcriptional regulator CusR (Fig. 1A). A positive regulation has then been assumed for TCS controlling periplasmic $Cu^+$. Supporting this model, deletion of either the SHK CusS or the RR CusR leads to a reduced tolerance to external $Cu^{2+}$, increased intracellular $Cu^+$, and lack of transcriptional activation of regulated genes (e.g., *cusC*) (24–27).

The regulons controlled by the canonical $Cu^+$-responsive TCS are limited to gene systems coding for the RNDs CusCFBA (26), PcoABCDRSE (27), and CopABCDRS (34, 35). However, $Cu^+$ homeostatic pathways do not behave as evolutionary units. Instead, distinct species assemble different repertoires of metal handling proteins to achieve periplasmic $Cu^+$ homeostasis (21). In particular, the *P. aeruginosa* CopRS regulon includes genes coding for an outer membrane transporter (PcoB), a multicopper oxidase (PcoA), and auxiliary proteins (PtrA, PA2807, and QueF) whose role in periplasmic $Cu^+$ distribution is still unclear (44–46) (Fig. 1B). Interesting, the *P. aeruginosa* CusCBA

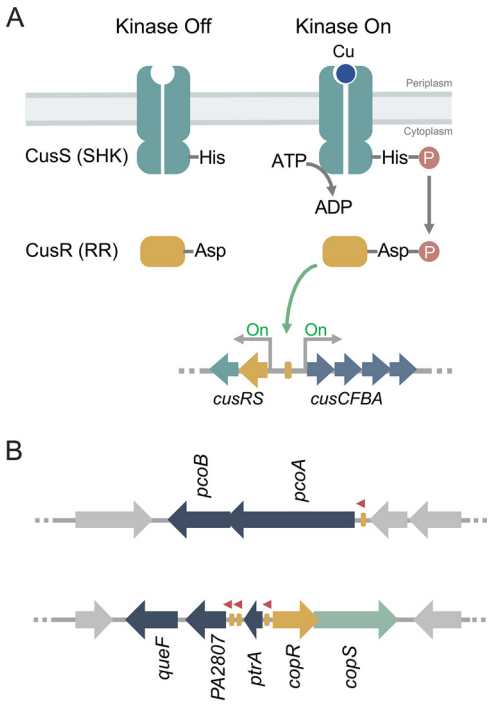


**FIG 1** Transcriptional control mediated by TCSs. (A) Activation dynamics of canonical TCSs exemplified with the *E. coli* Cu-sensing CusRS. (B) Scheme of the TCS *P. aeruginosa* CopRS regulon. Promoter regions recognized by CopR (yellow rectangles) and transcription direction (red arrowheads) are shown. Overlapping arrows indicate that the start codon of second gene overlaps the stop codon of first gene in both *pcoAB* and *copRS* operons.

transporter is not part of the CopRS regulon but is rather controlled by the cytoplasmic $Cu^+$ sensor CueR (9). Given the distinct architecture of the *P. aeruginosa* CopRS regulon, a distinct sensing/activating mechanism for the control of periplasmic $Cu^+$ homeostasis in *Pseudomonas* could be expected.

The structure of the isolated periplasmic domain of *E. coli* CusS shows four $Ag^+$ (acting as $Cu^+$ analog) binding sites per dimer (47). Two sites are symmetrically located at the dimer interface, and two are situated in outer loops of separated monomers. Reported estimates of metal-sensor affinities are limited and quite dissimilar among the different Cu-sensor histidine kinases. The *E. coli* CusS interacts with $Ag^+$ with an affinity in the micromolar range (48), while *Synechocystis* CopS binds $Cu^{2+}$ with high subattomolar affinity (32). Thus, significant aspects of sensor activation such as selectivity ($Cu^+$ versus $Cu^{2+}$) and sensitivity (affinity) are still undefined. These parameters will determine the level of free Cu in the periplasm and provide evidence for the metal redox status.

Here, we report that the transcriptional control of the CopRS regulon in *P. aeruginosa* relies on the Cu-dependent phosphatase activity of CopS, rather than on its kinase activity. Phosphorylation of the RR CopR and the consequent activation of the CopRS regulon appear independent of CopS. However, in the absence of Cu, CopS shuts down the transcriptional response to $Cu^+$, likely dephosphorylating CopR. Then, when the periplasmic $Cu^+$ level rises, the phosphatase activity of CopS is blocked, allowing the accumulation of phosphorylated CopR (CopR~P) which promotes the expression of the periplasmic $Cu^+$-homeostasis network. Finally, CopS binds both $Cu^+$ and $Cu^{2+}$ with similar high affinities, ensuring the absence of free Cu in the periplasm.

## RESULTS

CopRS controls *P. aeruginosa* periplasmic $Cu^+$ homeostasis (9). Notably, there are significant differences between the CopRS regulon and those of other characterized

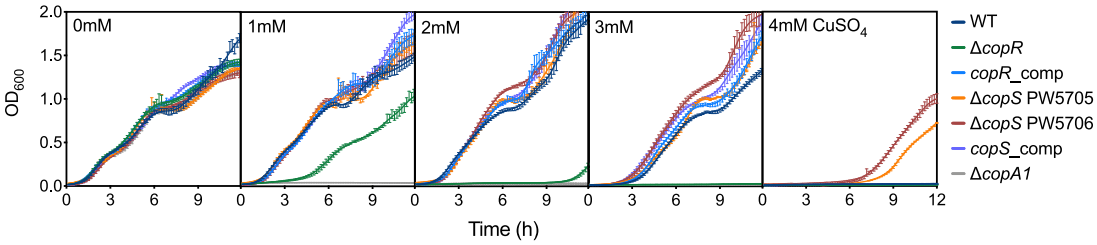


**FIG 2** Cu tolerance of Δ*copR* and Δ*copS* mutant strains. Growth rate of WT, Δ*copR*, Δ*copS* (PW5705 and PW5706), Δ*copA1*, and CopR and CopS complemented strains in the absence or the presence of increasing (0 to 4 mM) concentrations of $CuSO_4$. Data are the mean ± SEM from at least three independent experiments.

$Cu^+$-sensing TCSs, e.g., *E. coli* CusRS. The likely presence of additional mechanistic and molecular differences warranted a closer examination of CopRS function.

**Deletion of *copS* leads to Cu tolerance.** We initiated our studies by looking at the growth rate of Δ*copS* and Δ*copR* mutant strains in the presence of external $Cu^{2+}$. Based on the mechanism of described $Cu^+$-sensing TCSs (Fig. 1A), it was expected that the lack of either CopS or CopR would lower the cellular tolerance to external $Cu^{2+}$. As anticipated, the Δ*copR* strain was more susceptible to $Cu^{2+}$ than the wild-type (WT) strain (Fig. 2). In contrast, two independent *copS* transposon mutants, PW5705 and PW5706 (see Fig. S1 in the supplemental material), were surprisingly much more tolerant to external $Cu^{2+}$ than the WT strain. As these phenotypes were reversed by complementation with the corresponding gene, all subsequent experiments were performed with the Δ*copS* PW5706 strain. For comparison, in addition to the WT strain, the well-characterized $Cu^+$-sensitive Δ*copA1* mutant strain was included as a control in this initial phenotypical characterization (8).

Importantly, these growth phenotypes were the consequence of significantly different levels of intracellular $Cu^+$ upon exposure to $CuSO_4$ (Fig. 3). Thus, the Δ*copR* mutant strain accumulated more $Cu^+$, while the Δ*copS* cells stored less metal, than the WT strain. Again, alterations in $Cu^+$ levels were reversed by gene complementation of the mutant strains. These differences in Cu tolerance and cellular metal levels observed for the Δ*copR* and Δ*copS* mutant strains cannot be explained by the currently accepted model derived from the *E. coli* TCS CusRS (Fig. 1A) and suggest an alternative mechanism for coupling periplasmic $Cu^+$ sensing and gene expression in *P. aeruginosa*.

**The CopRS regulon is expressed in the Δ*copS* mutant strain independently of the $Cu^+$ levels.** Toward understanding the increased Cu tolerance and intracellular levels in the Δ*copS* strain, we investigated the transcriptional response to $Cu^{2+}$ exposure of the CopRS regulon in the Δ*copR* and Δ*copS* mutant strains. We have described that CopRS controls the expression of *pcoA*, *pcoB*, *ptrA*, *queF*, and *PA2807* coding for periplasmic and outer membrane proteins (Fig. 1B) (9). As previously observed in the WT strain, genes of the CopRS regulon are induced in response to external $Cu^{2+}$ exposure (Fig. 4). As expected, their Cu-induced expression was abolished in the Δ*copR* mutant. In contrast, the Δ*copS* mutant strain showed a constitutive activation of all the genes of the CopRS regulon, even in the absence of the $Cu^{2+}$ stimulus. In the Δ*copS* background, expression of these genes was maximal and independent of the presence of $Cu^{2+}$ in the culture medium. That similar expression pattern of the CopRS-activated genes in the Δ*copS* strain was attained in the absence of added $Cu^{2+}$ and in the presence of low, nondeleterious $Cu^{2+}$ levels (0.5 mM), intermediate toxic $Cu^{2+}$ levels (2 mM), and lethal $Cu^{2+}$ levels (4 mM) (Fig. S2). This suggests that CopS is not required to activate, i.e., phosphorylate, CopR. The activation of CopR in the Δ*copS* mutant in the absence of supplemented $Cu^{2+}$ points to a mechanism where the phosphatase activity of CopS maintains low levels of CopR~P under noninducing conditions. The Δ*copS* strain failure to maintain the system *off* in the absence of added Cu was reversed in the complemented strain (Fig. 4). The transcriptional analyses also showed that the expression of the *copRS* operon is not autoregulated (Fig. S3). That is, even

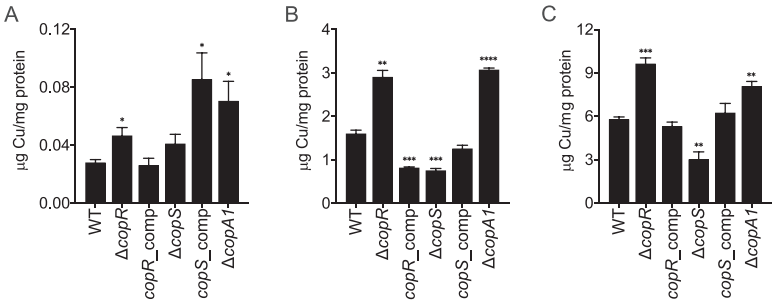


**FIG 3** Whole-cell Cu levels in WT, Δ*copR*, Δ*copS*, Δ*copA1*, and CopR and CopS complemented strains under normal growth conditions (i.e., no additional $CuSO_4$ added) (A) and after 10 min exposure to 2 mM $CuSO_4$ (B) or 4 mM $CuSO_4$ (C). Data are the mean ± SEM from three independent experiments. Significant differences from values with the WT strain as determined by unpaired two-tailed Student's *t* test are *, $P < 0.05$; **, $P < 0.01$; ***, $P < 0.001$; ****, $P < 0.0001$.

though *copRS* expression is induced in response to $Cu^+$, it was not affected either in the Δ*copR* or in the Δ*copS* mutant strain. Noticeably, the repressed transcription of *oprC*, coding for the outer membrane Cu importer (9, 49), was further repressed in the Δ*copS* mutant strain, consistent with the $Cu^+$-tolerant phenotype, i.e., less intracellular Cu, exhibited by this strain (Fig. S4A). Conversely, the increased transcription of genes in the CueR regulon (*copA1* and *cusA*) in response to $Cu^+$ was not altered either in the Δ*copR* or in the Δ*copS* mutant strain (Fig. S4B). This confirms that the lack of transcriptional control observed in the Δ*copR* and Δ*copS* mutant strains is limited to the genes of the CopRS regulon. Maximal transcription of the CopRS-activated genes in the Δ*copS* strain, even in the absence of external $Cu^{2+}$ stress, requires CopR∼P. As mentioned before, RRs can be phosphorylated either by alternative kinases or metabolically, by physiologically relevant small phosphodonors like the acetyl phosphate pool (39–43). This pool, in turn, depends on the activity of two enzymes, the phosphate acetyltransferase Pta and the acetate kinase AckA. Testing the role of acetyl phosphate on

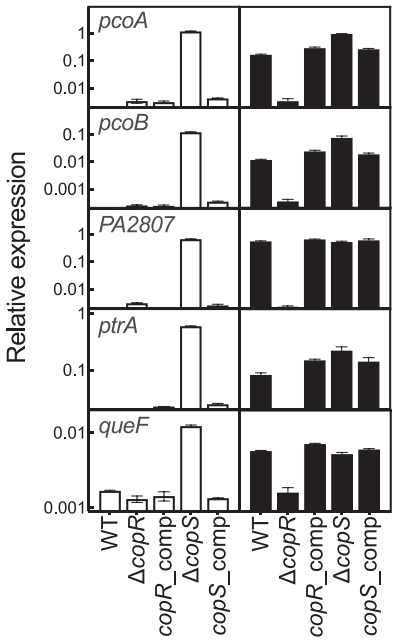


**FIG 4** Expression of genes in the CopRS regulon in WT, Δ*copR*, Δ*copS*, and corresponding complemented strains in the absence (white) and the presence (black) of 0.5 mM $CuSO_4$ (5-min treatment). Transcript levels of *pcoA*, *pcoB*, *PA2807*, *ptrA*, and *queF* genes are plotted relative to that of the housekeeping gene *PA4268*. Data are the mean ± SEM from three independent experiments.

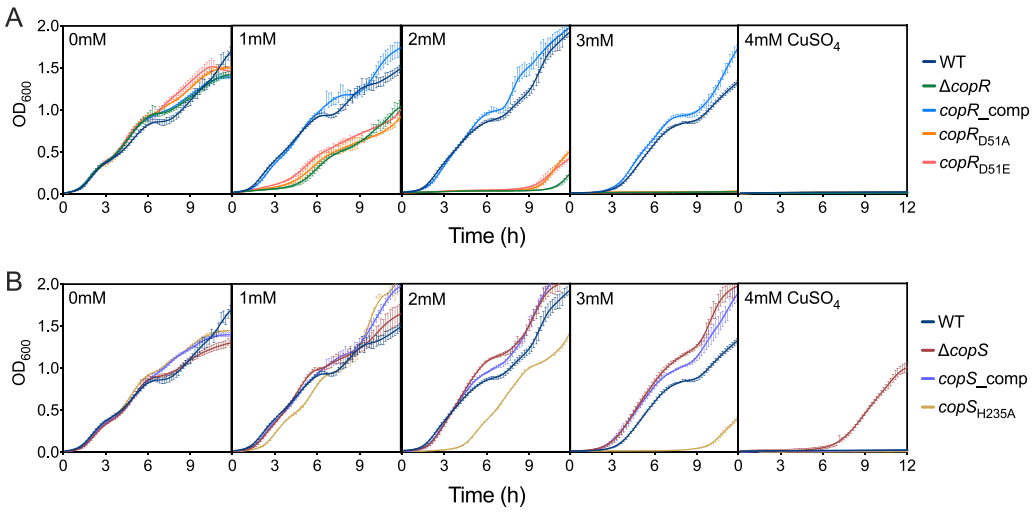


**FIG 5** Cu tolerance of Δ*copR* and Δ*copS* mutant strains complemented with CopR and CopS mutant proteins lacking the phosphorylatable residues. (A) Growth rate of the Δ*copR* mutant complemented with $copR_{D51A}$ or $copR_{D51E}$ in the absence or the presence of increasing (0 to 4 mM) concentrations of $CuSO_4$. (B) Growth rate of the Δ*copS* mutant complemented with $copS_{H235A}$ in the presence of 0 to 4 mM $CuSO_4$. Data are the mean ± SEM from three independent experiments.

CopR phosphorylation, the $Cu^{2+}$ resistance of the Δ*pta* and Δ*ackA* strains was evaluated (Fig. S5). Both strains showed a $Cu^{2+}$ sensitivity profile similar to that of the WT strain, suggesting that phosphorylation of CopR does not depend on the acetyl phosphate pool and the involvement of a yet-unidentified SHK.

**$His_{235}$ acts as a switch to turn on/off the CopS signaling pathway.** The cytoplasmic region of the SHK sensory proteins contains the catalytic domain and the phosphotransfer domain able to switch between kinase and phosphatase activities in a signal-dependent manner (42, 50). In most SHKs, this phosphotransfer domain contains an invariant His residue that autophosphorylates in the first step of the signaling cascade, activating the kinase state of the SHK. Subsequently, the RR protein is phosphorylated in a highly conserved phosphoacceptor Asp, leading to the transcriptional induction of its activated genes (51) (Fig. 1A). In contrast to the kinase state, in the phosphatase state a dephosphorylated SHK removes the phosphate group from the RR (42). The kinase and phosphatase states are mutually exclusive. In some cases, the activation of the kinase state is associated with phosphatase deactivation with the consequent accumulation of phosphorylated RR. The observed phenotypes in Δ*copS* and Δ*copR* strains suggest that in the absence of $Cu^{+}$, CopS acts as a phosphatase dephosphorylating CopR∼P. Then, when CopS senses $Cu^{+}$, its phosphatase would be inactivated, leading to a rise of CopR∼P, triggering the expression of the CopRS regulon. Testing these ideas, the phosphorylatable residues, $His_{235}$ in CopS and $Asp_{51}$ in CopR, were identified by sequence alignment with characterized TCS (Fig. S6). Site-directed mutagenesis was performed to generate $Asp_{51}$Ala and $Asp_{51}$Glu replacements in CopR and $His_{235}$Ala in CopS coding sequences, and the resulting constructs were employed to complement the corresponding Δ*copR* and Δ*copS* mutant strains.

Figure 5A shows that the mutations $Asp_{51}$Ala and $Asp_{51}$Glu in CopR lead to growth phenotypes comparable to that of the Δ*copR* strain. This pointed to the requirement of Asp at this position for CopR function and revealed that the Glu residue does not act as a phosphomimetic residue. In agreement, Fig. 6 shows that neither $CopR_{D51A}$ nor $CopR_{D51E}$ was able to activate *pcoB* expression in the presence of external $Cu^{2+}$, a lack of function associated with the absence of the $Asp_{51}$ phosphorylation. Conversely, the $His_{235}$Ala CopS mutant behaved differently from both the WT and the Δ*copS* strain. In contrast to the $Cu^{2+}$ tolerance phenotype observed for the Δ*copS* mutant, the $His_{235}$Ala CopS mutant had an increased sensitivity to $Cu^{2+}$ (Fig. 5B), suggesting that the phosphatase activity of CopS remains functional in the absence of $His_{235}$. Analysis

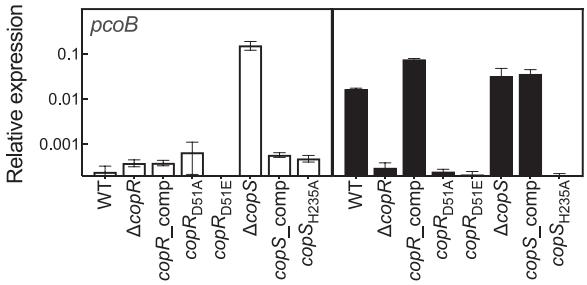


**FIG 6** Expression of *pcoB* in Δ*copR* and Δ*copS* mutant strains complemented with CopR and CopS lacking the phosphorylatable residues. *pcoB* expression was determined in the absence (white) and the presence (black) of 2 mM $CuSO_4$ (5-min treatment) in the indicated strains. The Δ*copR* mutant was complemented with *copR* coding for substitutions $Asp_{51}Ala$ and $Asp_{51}Glu$. The Δ*copS* mutant was complemented with the *copS* gene coding for substitution $His_{235}Ala$. Transcript levels of *pcoB* are plotted relative to the housekeeping gene *PA4268*. Data are the mean ± SEM from three independent experiments.

of the transcriptional activation of genes in the CopRS regulon further supports this idea. In the absence of supplemented $Cu^{2+}$, *pcoB* transcription remained low in the $His_{235}Ala$ CopS mutant, similar to the level observed in the WT strain and in contrast to the increased expression in the Δ*copS* mutant strain. In fact, addition of external $Cu^{2+}$ did not promote the transcription of *pcoB* in the $His_{235}Ala$ mutant, similar to the *pcoB* expression pattern in the Δ*copR* strain and clearly different from the induction observed in the WT and the maximal expression attained in the Δ*copS* mutant. The more marked *pcoB* expression defect under Cu stress of the $copS_{H235A}$ strain compared to the Δ*copR* strain is likely associated with experimental conditions. Importantly, the lack of transcriptional activation of *pcoB* suggests that the $His_{235}Ala$ CopS mutant was not able to respond to changes in periplasmic $Cu^{+}$ levels, explaining the $Cu^{2+}$-sensitive phenotype observed for this strain (Fig. 5B) and suggesting that the $His_{235}Ala$ mutation locked CopS in a phosphatase-ON state irresponsive to the presence of Cu.

**CopS periplasmic sensor domain binds two $Cu^{+}$ ions per functional unit.** Most TCS sensors are homodimeric membrane proteins. The periplasmic sensor domain of CopS, flanked by two transmembrane segments (Fig. S1), extends between residues 34 and 151 [$CopS_{(34–151)}$]. The function of the system relies on its ability to bind cognate metal ions. To explore CopS metal binding properties, the *P. aeruginosa* $CopS_{(34–151)}$ sensor domain carrying alternative His or Strep tags was heterologously expressed and purified to homogeneity (Fig. S7). His-tagged proteins were used in $Cu^{+}$ binding, while the Strep-tagged fragments were used in $Cu^{2+}$ binding experiments.

The $Cu^{+}$ binding stoichiometry of the isolated domain was first measured at a saturating metal concentration (five times molar excess) in the presence of dithiothreitol (DTT) as reducing agent. The $CopS_{(34–151)}$ dimer was able to bind 2.3 ± 0.5 $Cu^{+}$. This differs from the stoichiometry of four $Ag^{+}$ (used as $Cu^{+}$ analog) per dimer observed in *E. coli* CusS (47). However, the periplasmic sensor domain of CopS homolog proteins is considerably shorter than the CusS domain, lacking a loop containing residues ($Ser_{84}$, $Met_{133}$, $Met_{135}$, and $His_{145}$) involved in metal binding in CusS (Fig. S6B). In effect, a phylogenetic tree built with sequences homologous to CopS and CusS (>45% identity) shows a clear evolution of two distinct subgroups of CusS homologs in *Enterobacterales* and in *Burkholderiales* and a separate group of CopS homologs in *Pseudomonadales* (Fig. S8). This structural difference leading to the alternative stoichiometry can be more easily observed when the homology modeling of *P. aeruginosa* CopS is overlapped with the crystal structure of the $Ag^{+}$-bound periplasmic sensor domain of *E. coli* CusS (47) (Fig. 7). The two symmetric metal binding sites fully conserved in both CopS and CusS are located at the dimeric interface. Each site is formed by two invariant His residues ($His_{41}$ and $His_{140}$ in CopS), one from each dimer subunit. A Phe residue likely interacting with the metal in CusS is also conserved in CopS ($Phe_{42}$). These are probably the $Cu^{+}$-sensing

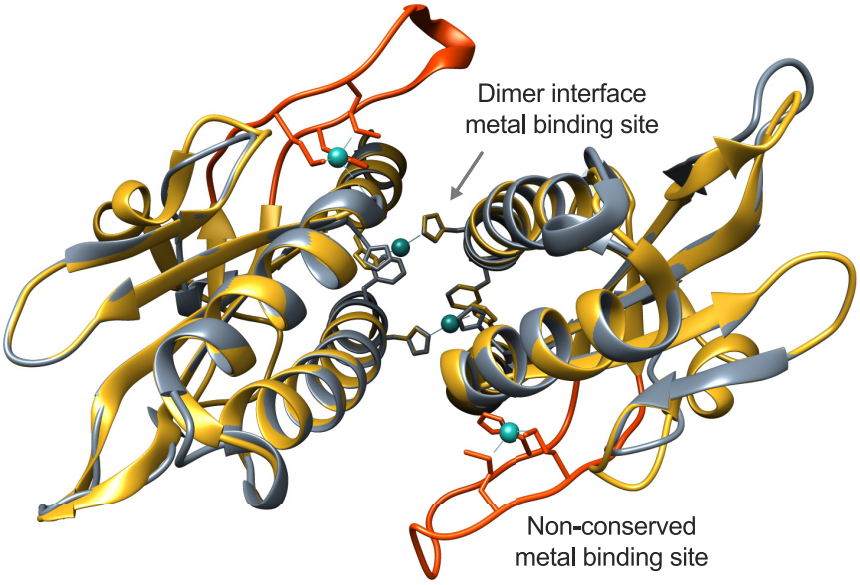


```
CopS_PA01       -MSAGFGSRMSLGVRLSLLFAACTAAVSLIAGLIFSRAIDEHFVELDHMAMSAKLAV---    56
CusS_Ecol       MVSKPFQRPFSLATRLTFFISLATIAAFFAFAWIMIHSVKVHFAEQDINDLKEISATLER    60
                 :*  *   :**..**:::::: .* *. :  . *: :::. **.* *   :.   *.

CopS_PA01       ---------------FRDELRGLG--------SEQQ---MRRREAELLRELARHPDLGLRL    91
CusS_Ecol       VLNHPDETQARRLMTLEDIVSGYSNVLISLADSQGKTVYHSPGAPDIREFTRDAI--PDK    118
                              :.* : * .       ..*     :   *  :**::*.

CopS_PA01       NGPDGNLWFERLPQPAHPGL-------PANRELGAPLEPGNDASPRLTV--ILDISHHQH    142
CusS_Ecol       DAQGGEVYLLSGPTMMMPGHGHGHMEHSNWRMINLPVGPLVDGKPIYTLYIALSIDFHLH    178
                :. .*::::   *    **          * :. *: *  *..*  *:   *.*..* *
```

**FIG 7** Structural superposition of the periplasmic $Cu^+$ binding loop of *P. aeruginosa* CopS (gray) and *E. coli* CusS (yellow). The structure of CopS was modeled using the CusS structure as the template (PDB ID: 5KU5 [43]). An overall root mean square deviation of 0.791 Å (C$\alpha$ atoms) was calculated for the superposition of CopS and CusS structures. Conserved Cu binding sites at the dimeric interface ($His_{41}$, $Phe_{42}$, and $His_{140}$) are shown as sticks in the structural model and highlighted in yellow in the sequence alignment. The $Cu^+$ binding sites within the CusS orange loops (framed in rectangle in the alignment) are not conserved in CopS.

sites involved in signal transduction. On the other hand, the structural comparison clearly shows that the loop containing the additional metal binding sites of CusS is missing in CopS (orange loops, Fig. 7).

**The CopS periplasmic sensor binds Cu ions with femtomolar affinities.** By analogy with how cytoplasmic sensor metal affinities are tuned to maintain free metal levels (52, 53), the affinity of CopS for $Cu^+$ ions will certainly have determinant effects on free (hydrated) $Cu^+$ ion levels in the periplasm. Exploring the binding of $Cu^+$ to CopS, we measured the sensor metal binding affinity using competing ligands. The ligands were present in excess to ensure effective competition. In all cases, the determinations were performed assuming that both Cu sites at the CopS dimer interface were functionally independent and thermodynamically indistinguishable. Initial determinations of $CopS_{(34–151)}$ affinity for $Cu^+$ using bathocuproine disulfonate (BCS) as a competitor showed a limited but measurable decrease in the absorbance of the $[Cu^I(BCS)_2{}^{3-}]$ complex, corresponding to a $K_D$ (dissociation constant) value of $CopS_{(34–151)}$ for $Cu^+$ of $2.2 \times 10^{-14}$ M (data not shown). However, it was apparent that CopS was not an effective competitor with BCS for the metal. Instead, 2,2′-bicinchoninic acid (BCA), with a lower affinity for copper than that of BCS, appeared more appropriate to measure affinities in the femtomolar range (54). Using BCA as the competing ligand and fitting titration curves to equation 2, a $CopS_{(34–151)}$-$Cu^+$ $K_D$ of $(2.77 \pm 0.07) \times 10^{-14}$ M

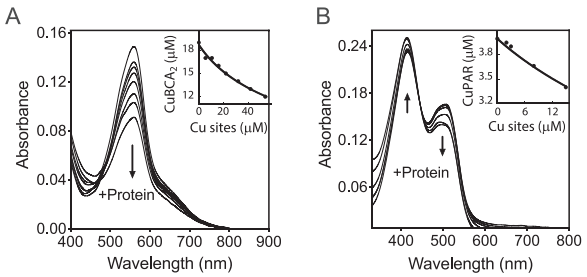


**FIG 8** Determination of the dissociation constants $K_D$ of the periplasmic Cu binding loop of $CopS_{(34–151)}$. (A) Spectrophotometric titration of 100 $\mu$M BCA and 18.7 $\mu$M $Cu^+$ with 10 to 50 $\mu$M His-tagged $CopS_{(34–151)}$. The arrow indicates the decrease in absorbance at 562 nm upon protein addition. The inset shows the fitting of the data set to equation 2 with a $K_D$ of $(2.77 \pm 0.07) \times 10^{-14}$ M ($R^2$ 0.992). Two Cu sites per CopS dimer are assumed. (B) Spectrophotometric titration of 10 $\mu$M PAR and 4 $\mu$M $Cu^{2+}$ with 2 to 20 $\mu$M Strep-tagged $CopS_{(34–151)}$. The arrows indicate the increase in absorbance at 415 nm and the decrease at 562 nm upon protein addition. The inset shows the fitting of the data set to equation 4 with a $K_D$ of $(3.3 \pm 0.1) \times 10^{-14}$ M ($R^2$ 0.984).

was obtained (Fig. 8A). This appears within the range of affinities observed for many other $Cu^+$ binding molecules (11, 54, 55).

*Synechocystis* CopS binds $Cu^{2+}$ with high subattomolar affinity ($Cu^+$ binding stoichiometry was not reported) (32). Exploring the possibility of high-affinity $Cu^{2+}$ binding to *P. aeruginosa* CopS, the chromogenic ligand 4-(2-pyridylazo)resorcinol (PAR) was used as a competitive ligand for $Cu^{2+}$ with purified Strep-tagged $CopS_{(34–151)}$ (Fig. S7), in the absence of reducing agents. A $CopS_{(34–151)}$-$Cu^{2+}$ $K_D$ of $(3.3 \pm 0.1) \times 10^{-14}$ M was observed (Fig. 8B). Consequently, it is apparent that $CopS_{(34–151)}$ binds both $Cu^+$ and $Cu^{2+}$ with quite similar affinities in the femtomolar range. These high affinities provide insights into the *in vivo* metal dynamics and virtual absence of free Cu ions in the bacterial periplasm.

## DISCUSSION

The relevance of the periplasmic Cu pool in the *P. aeruginosa* response to $Cu^{2+}$ stress is well established (10, 56). Results presented here show novel important characteristics of the *P. aeruginosa* TCS CopRS. The sensor has a negative-control mechanism based on its phosphatase rather than on its kinase activity. At the dimer interface, it binds two $Cu^{+/2+}$ ions with femtomolar affinities, likely resulting in the absence of periplasmic free Cu. This CopRS distinct $Cu^+$ signaling mechanism is in line with the other unique features of the *P. aeruginosa* Cu homeostasis network, namely, cytoplasmic and periplasmic sensors with singular regulons, an RND-transporter regulated by the cytoplasmic sensor, and multiple cytoplasmic $Cu^+$ chaperones and efflux $P_{1B}$-ATPases (8–11, 57). The emerging model challenges a number of ideas associated with early studies of the *E. coli* CusRS TCS. Along with *Salmonella*, which has distinct $Cu^+$ balance mechanisms (6), *P. aeruginosa* provides a clear example of alternative approaches used by bacteria to achieve Cu homeostasis.

**CopS Cu-dependent phosphatase activity mediates signal transduction.** Characterization of CopRS was initiated by analyzing the tolerance of Δ*copS* and Δ*copR* strains to external $Cu^{2+}$. While an increased sensitivity was expected based on the reported phenotypes of *E. coli* Δ*cusS* and Δ*cusR* strains, the Δ*copS* strain showed higher tolerance to external $Cu^{2+}$. Although unexpected, this phenomenon has been previously observed, albeit unnoticed. It was reported that deletion of the *P. aeruginosa* CopS did not compromise the ability of the bacteria to grow in the presence of $Cu^{2+}$ (58). Furthermore, there was no evident Cu-induced expression of a *lacZ* transcriptional fusion to a *Pseudomonas putida* CinRS (a CopRS ortholog)-dependent promoter in a *P. aeruginosa* Δ*copR* background. However, Cu-independent expression of the same reporter was attained in the *P. aeruginosa* Δ*copS* background (59). Also similar to the *P.*

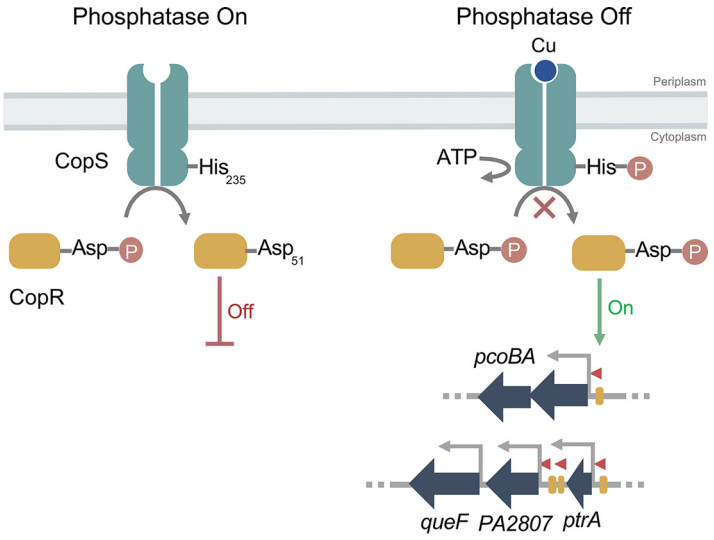


**FIG 9** Model of the phosphatase-based mechanism of the *P. aeruginosa* CopRS. Phosphatase On: when periplasmic free Cu remains under the subfemtomolar level, the CopS phosphatase activity maintains low levels of phosphorylated CopR, shutting *off* the transcriptional response to high periplasmic Cu. Phosphatase Off: upon Cu binding, CopS autophosphorylates at $His_{235}$. This turns *off* the CopS phosphatase activity, allowing the accumulation of phosphorylated CopR and triggering the expression of the CopRS regulon (i.e., *pcoA*, *pcoB*, *queF*, *PA2807*, and *ptrA*).

*aeruginosa* Δ*copS* strain, a *P. fluorescens* Δ*copS* strain was more tolerant to external $Cu^{2+}$ (36).

The $Cu^{2+}$ resistance phenotype of the *P. aeruginosa* Δ*copS* strain is supported by the maximal expression of the CopRS regulon and the consequent reduced whole-cell $Cu^{+}$ content. The simplest explanation for these observations is a mechanism where, in the absence of Cu, the CopS phosphatase activity abrogates the induction of the CopRS regulon by maintaining low levels of CopR∼P (Fig. 9). When CopS detects periplasmic Cu overload, its phosphatase activity is blocked allowing the accumulation of CopR∼P, which promotes the expression of the periplasmic Cu homeostasis network.

Signal transduction by archetypical TCSs relies on bifunctional kinase/phosphatase SHKs (60). A positive action results from sensor autokinase activity and phosphotransfer to the RR while negative regulation involves the sensor phosphatase activity (50). The ultimate determining factor of the cascade activation is the phosphorylation status of the RR. Accumulation of RR∼P is the consequence of a signal-dependent stimulation of the sensor-kinase activity or a signal-dependent blockage of the sensor-phosphatase activity. While we cannot rule out the absence of autokinase activity, or sensor phosphorylation by an alternative kinase, the most parsimonious model to explain our data is that CopS, under our experimental conditions, harbors autokinase and phosphatase activities. The signal-independent activation of the CopRS regulon in the Δ*copS* background evidences the requirement of the CopS phosphatase activity to maintain low levels of CopR∼P in the absence of Cu. It is also apparent that CopS is not required for the phosphorylation of CopR, implying that an alternative mechanism for the phosphorylation of CopR should exist. There is extensive evidence that RRs can be phosphorylated (cross-phosphorylated) by endogenous phosphodonors (39, 41–43). In the case of CopR, acetyl phosphate does not seem to be the donor. Alternative mechanisms for RR phosphorylation known as many-to-one or one-to-many, where many SHKs phosphorylate a given RR or a single SHK phosphorylates multiple RRs, have been proposed (38, 60). It could then be argued that CopR phosphorylation might be the consequence of an unspecific cross talk with a noncognate SHK that occurs only in the absence of CopS. However, such cross talk has been observed only when both the

reciprocal RR and the cognate SHK were absent (41). These conditions are distinct from those in our experiments.

The evidence indicates that Cu-dependent CopS autokinase activity, or at least the integrity of $His_{235}$, is required for the inhibition of the CopS-phosphatase activity. $His_{235}$Ala replacement leads to a $Cu^{+}$-independent inactivation of the regulon, suggesting a constitutively active phosphatase activity. While this points out that $His_{235}$ is not required for the CopS phosphatase activity, it implies that Cu-dependent CopS autophosphorylation turns *off* the CopS phosphatase activity, leading to accumulation of CopR∼P. That is, as described previously, the dephosphorylated SHKs have phosphatase activity (42, 50).

**CopS binds two Cu ions with femtomolar affinities.** Its Cu binding characteristics are what defines the function of CopS. We determined that *P. aeruginosa* CopS binds two metal ions with an affinity in the $3 \times 10^{-14}$ M range. Little information is available regarding the binding stoichiometry and affinities of other Cu-sensing TCS sensors. The structure of *E. coli* CusS clearly supports a stoichiometry of four metal atoms per CusS-sensing dimer (47). Two of these ions bind at the dimer interface, while the other two attach to external loops, one in each subunit. Structural comparison of *P. aeruginosa* CopS and *E. coli* CusS shows that both types of sensors would bind and sense the metal with conserved His residues at the dimer interface. However, the CusS extra sites are not conserved in CopS or in its homologs. Regarding binding affinities, *E. coli* CusS binds $Ag^{+}$ with a reported 8 $\mu$M affinity, measured in equilibrium dialysis experiments (48); in contrast, *Synechocystis* CopS binds $Cu^{2+}$ with subattomolar affinity (32). It would be quite speculative to compare such dissimilar determinations. However, it might be instructive to consider the observed $10^{-19}$ to $10^{-21}$ M affinities of cytoplasmic copper sensors in general (55, 61) and those determined for the cytoplasmic triad CopZ2/CueR/CopZ1 of *P. aeruginosa*, with relative affinities for $Cu^{+}$ ranging between $10^{-15}$ and $10^{-17}$ M (9, 11). The weaker affinity of CopS than of the cytoplasmic regulators and chaperones is likely the consequence of a metal binding site formed by His rather than Cys residues. This is a logical arrangement, given the possible oxidation of proximal Cys under periplasmic redox stress. Importantly, a femtomolar affinity still supports the idea that there would not be free $Cu^{+/2+}$ in the cell periplasm, as shown for the cytoplasm (55, 62). However, the relative binding strength of CopS is likely to be linked to those of periplasmic $Cu^{+}$ chaperones that exchange metal with the sensor. That is, the proteins should be able to exchange the metal. However, as shown with cytoplasmic chaperone/sensor partners, the protein-protein binding affinity will have a significant effect in the final exchange constant (11).

CopS binds both $Cu^{+}$ and $Cu^{2+}$ with similar high affinities. It is accepted that cytoplasmic transporters and chaperones bind and distribute cuprous ions. However, the periplasm is a more oxidizing compartment (63, 64), containing enzymes such as the multicopper oxidase PcoA present in the periplasm of *P. aeruginosa* (65). It has been proposed that periplasmic enzymes might catalyze $Cu^{+}$ oxidation to the assumed less toxic $Cu^{2+}$ (66). However, free (hydrated) $Cu^{+}$ would be spontaneously oxidized by $O_2$ in an aerobic environment. Then, the redox status of periplasmic Cu is unclear and beyond the goals of this report. We presume that Cu oxidation state will depend on the molecule interacting with and delivering Cu to CopS. In any case, the capability to bind both $Cu^{+}$ and $Cu^{2+}$ might help CopS to sense the metal under redox stress.

**The distinct CopRS mechanism is in line with the singular architecture of the *P. aeruginosa* Cu homeostasis system.** *E. coli* and *Salmonella* are the frequent models to explore transition metal homeostasis in Gram-negative bacteria. However, recent studies of *P. aeruginosa* have begun to show different novel molecular strategies to sense, buffer, and distribute $Cu^{+}$ (8–10, 67). For instance, consider how the regulons of both compartmental sensors, CopRS and CueR, differ among these three organisms (6, 9, 24, 68, 69). Also, analyze the multiple functionally distinct homologous $Cu^{+}$ ATPases present in *Salmonella* and *Pseudomonas* and how these three Gram-negative bacteria have solved cytoplasmic $Cu^{+}$-chaperoning using alternative strategies (6, 11, 70). Along with these observations, the relevance of periplasmic $Cu^{+}$ sensing, storage, and transport

has become more apparent. Then, it is not surprising that these model systems solve periplasmic $Cu^+$ sensing either via a kinase sensor (CusRS, *E. coli*), an integration of a cytoplasmic Cu sensor with a general envelope stress response TCS (CueR-CpxRS, *Salmonella* [71]) or a phosphatase sensor (CopRS, *P. aeruginosa*). The evolutive and ecological advantages of these systems are still to be discovered and will be the subject of future enquiries in the field.

## MATERIALS AND METHODS

**Bacterial strains, plasmids, and growth conditions.** Bacterial strains, plasmids, and primers used in this study are listed in Table S1 in the supplemental material. *P. aeruginosa* PAO1 served as WT strain. Mutant strains PW5704 (Δ*copR*), PW5705 (Δ*copS*), PW5706 (Δ*copS*), PW2519 (Δ*pta*), and PW2520 (Δ*ackA*) were obtained from the *P. aeruginosa* PAO1 transposon mutant library (University of Washington, Seattle, WA) (72, 73). *P. aeruginosa* strains were grown at 37°C in Luria-Bertani (LB) medium supplemented with 25 $\mu$g/ml Irgasan, 30 $\mu$g/ml tetracycline (mutant strains), or 30 $\mu$g/ml gentamicin (complemented strains). *E. coli* strains were grown at 37°C in LB medium supplemented with 100 $\mu$g/ml ampicillin, 30 $\mu$g/ml kanamycin, or 10 $\mu$g/ml gentamicin, depending on the plasmid selection.

**Construction of *P. aeruginosa* complemented strains.** Mutant strains were complemented with the corresponding gene under the control of the native promoter using the mini-Tn7T insertion system (74). Briefly, the genes and their 500-bp upstream promoter regions were amplified by PCR. The 3′ primer included a $His_6$ tag coding sequence. Amplicons were cloned into the pUC18-mini-Tn7T-Gm suicide delivery vector. These plasmids were used as the template to introduce mutations coding for single substitutions $copR_{D51A}$, $copR_{D51E}$, and $copS_{H235A}$ using Gibson assembly (75). The resulting plasmids were then introduced into recipient strains by conjugation, using the helper strains SM10(λpir)/pTNS2 and HB101/pRK2013. Conjugants were selected on 30 $\mu$g/ml gentamicin-25-$\mu$g/ml Irgasan-LB plates. Complemented strains were verified by PCR.

**$Cu^{2+}$ sensitivity assay.** Overnight cultures were diluted in 25 $\mu$g/ml Irgasan-LB medium, adjusted to an optical density at 600 nm ($OD_{600}$) of 0.05, and supplemented with the indicated $CuSO_4$ concentration. Cell growth in 0.2 ml liquid medium was monitored for 24 h ($OD_{600}$) at 37°C with continuous shaking using an Epoch 2 microplate spectrophotometer (BioTek).

**Whole-cell Cu content.** Cells (mid-log phase) were incubated in LB medium supplemented with 0.5, 2, or 4 mM $CuSO_4$. Aliquots were taken after 10 min, treated with two times molar excesses of DTT and BCS, and harvested by centrifugation at 17,000 × *g*, 1 min. Pellets were washed twice with 150 mM NaCl and mineralized with fuming $HNO_3$ (trace metal grade) for 60 min at 80°C and 2 M $H_2O_2$ for 60 min at room temperature. Cu levels were measured using atomic absorption spectroscopy (AAS) as described previously (9).

**Gene expression analysis.** Cells (mid-log phase) were incubated in antibiotic-free LB medium supplemented with 0.5, 2, or 4 mM $CuSO_4$. In all cases, 0.5-ml aliquots were taken at 5 min and stabilized with RNAprotect bacterial reagent (Qiagen), and RNA was isolated with the RNeasy minikit (Qiagen). RNA was treated with DNase I, purified by phenol-chloroform extraction, and ethanol precipitated. One microgram of RNA was used for cDNA synthesis using the ProtoScript II kit (New England BioLabs). qPCRs were carried out with FastStart Essential DNA Green Master (Roche) in a 10-$\mu$l final volume, using 0.25 $\mu$M (each) primer (Table S1). The efficiency of primer sets was evaluated by qPCR in serial dilutions of WT cDNA. Results were normalized to 30S ribosomal protein S12 (*PA4268*) (8).

**Protein expression and purification.** The DNA fragment encoding the periplasmic copper binding loop of $CopS_{(34–151)}$ was amplified from genomic DNA using 3′-end primers that introduced sequences encoding either a Strep tag or a $His_6$ tag joined by a tobacco etch virus (TEV) cleavage site (Table S1). The His-tagged protein had a higher expression yield and was used in $Cu^+$ binding experiments since this tag does not bind monovalent $Cu^+$. However, the His tag binds $Cu^{2+}$. Cleavage of the His tag was not pursued because the CopS (dimer) and the TEV have exactly the same molecular weight and it is not possible to ensure full cleavage. In consequence, a Strep-tagged protein was used in $Cu^{2+}$ binding experiments. Resulting amplicons were cloned in the pBAD-topo vector (Invitrogen) and expressed in *E. coli* LMG194 cells. His-tagged $CopS_{(34–151)}$ was purified using Ni-NTA columns (Roche) (11). Strep-tagged $CopS_{(34–151)}$ was affinity purified using Strep-Tactin XT Superflow columns (IBA) (11). Purified proteins were stored in 20% glycerol, 25 mM Tris (pH 8), 100 mM sucrose, 150 mM NaCl at −80°C. Protein concentrations were determined in accordance with work of Bradford (76), and purity was estimated by SDS-PAGE followed by Coomassie brilliant blue staining (Fig. S7). Proteins were purified as ≥90% *apo* forms as confirmed by AAS.

**Copper binding determinations.** $CopS_{(34–151)}$-$Cu^+$ binding stoichiometry was determined by incubating $CopS_{(34–151)}$ His-tagged protein with five times molar excess of $CuSO_4$ in 25 mM HEPES, pH 8, 150 mM NaCl, 0.5 mM DTT for 10 min at room temperature with gentle agitation. DTT was included to reduce $Cu^{2+}$ to $Cu^+$ and prevent protein precipitation that occurs upon addition of excess $Cu^+$ using ascorbate. This is a common observation when purified proteins are exposed to Cu and is usually solved, as in this case, by replacing the reducing agent. Unbound $Cu^+$ was removed by passage through a Sephadex G-10 column (GE Healthcare) followed by two washing steps using a 3-kDa Centricon. The amount of $Cu^+$ bound to protein was determined by AAS.

$CopS_{(34–151)}$-$Cu^+$ dissociation constants ($K_D$) were determined by competition assays with the chromogenic ligands BCS {$[Cu^I(BCS)_2]^{3-}$ $\beta_2'$ formation constant $10^{20.8}$ $M^{-2}$, $\varepsilon_{483\ nm}$ 13,000 $M^{-1}$ $cm^{-1}$} and BCA {$[Cu^I(BCA)_2]^{3-}$ $\beta_2'$ formation constant $10^{17.7}$ $M^{-2}$, $\varepsilon_{562\ nm}$ 7,900 $M^{-1}$ $cm^{-1}$ [77]}. $Cu^+$ solutions were

generated from $CuSO_4$ in the presence of large excess ascorbate and NaCl, which stabilizes $Cu^+$ as $[Cu^ICl_n]^{(17-n)-}$ (78). Briefly, for BCS competitions, 10 $\mu$M $Cu^+$, 25 $\mu$M BCS in buffer 25 mM HEPES, pH 8, 150 mM NaCl, 10 mM ascorbic acid were titrated with 10 to 50 $\mu$M His-tagged $CopS_{(34–151)}$ and incubated for 5 min at room temperature, and the 300- to 800-nm absorption spectra were recorded. The same protocol was used for BCA competitions using 18.7 $\mu$M $Cu^+$, 100 $\mu$M BCA, and 5 to 50 $\mu$M protein instead. $CopS_{(34–151)}$-$Cu^+$ $K_D$s were calculated by curve-fitting of the experimental data to the equilibrium in equations 1 and 2 (54).

$$MP + 2L' \leftrightharpoons ML_2 + P \tag{1}$$

$$K_D\beta_2' = \frac{\left([P]_{\text{total}}/[MP]\right) - 1}{\left\{\left([L]_{\text{total}}/[ML_2]\right) - 2\right\}^2 [ML_2]} \tag{2}$$

$CopS_{(34–151)}$-$Cu^{2+}$ $K_D$s were determined using the indicator PAR as competitor ([$Cu^{II}$(PAR)] conditional $K_A'$ formation constant for $Cu^{2+}$ at pH 7.4 of $10^{14.6}$ $M^{-1}$, isosbestic point $A_{445\ nm}$, $\varepsilon_{505\ nm}$ 41,500 $M^{-1}$ $cm^{-1}$ [79]). Four micromolar $Cu^+$, 10 $\mu$M PAR in buffer 20 mM HEPES, pH 7.4, 150 mM NaCl were titrated with 2 to 20 $\mu$M Strep-tagged $CopS_{(34–151)}$ and incubated at room temperature to equilibrate until no further spectral changes were observed (60 min), and the 300- to 800-nm absorption spectra were recorded. The $K_D$ value was obtained from a curve-fitting of a series of experimental data to equations 3 and 4. Reported errors are asymptotic standard errors provided by the fitting software (Kaleidagraph; Synergy).

$$MP + L' \leftrightharpoons ML + P \tag{3}$$

$$K_D K_A' = \frac{\left([P]_{\text{total}}/[MP]\right) - 1}{\left([L]_{\text{total}}/[ML]\right) - 1} \tag{4}$$

**Bioinformatic approaches.** In general, protein sequences were retrieved from UniProt (80) and aligned using Clustal Omega (81). To build the phylogenetic trees, the full-length protein sequences of *E. coli* CusS and *P. aeruginosa* CopS sequences were independently used as query to search for homologs in the UniProtKB database using the UniProt/BLAST tool. Sequences more than 45% identical over their entire lengths were retrieved and aligned. Phylogenetic trees were calculated with the Jalview software (82), using the distance matrix BLOSUM62 and the Average Distance (unweighted pair group method using average linkages [UPGMA]) algorithm.

The structure of the soluble periplasmic copper binding loop of $CopS_{(34–151)}$ was modeled using the online server SWISS-MODEL (83) and the structure of the *E. coli* CusS soluble periplasmic domain (PDB ID: 5KU5) (47) as the template. Conserved metal binding residues of CopS were identified by superimposing its structure with 5KU5 using UCSF Chimera (84).

## SUPPLEMENTAL MATERIAL

Supplemental material is available online only.

**FIG S1**, PDF file, 0.2 MB.

**FIG S2**, PDF file, 0.04 MB.

**FIG S3**, PDF file, 0.03 MB.

**FIG S4**, PDF file, 0.04 MB.

**FIG S5**, PDF file, 0.1 MB.

**FIG S6**, PDF file, 0.1 MB.

**FIG S7**, PDF file, 1.1 MB.

**FIG S8**, PDF file, 0.1 MB.

**TABLE S1**, PDF file, 0.1 MB.

## ACKNOWLEDGMENTS

This work was supported by grant R01GM114949 from the National Institutes of Health to J.M.A. F.C.S. is a career investigator of CONICET and the Rosario National University Research Council.

Author contributions: L.N.-A. and C.X. performed research; L.N.-A., F.C.S., and J.M.A. designed research, analyzed data, and wrote the paper.

We declare no competing interest.

## REFERENCES

1. Argüello JM, Raimunda D, Padilla-Benavides T. 2013. Mechanisms of copper homeostasis in bacteria. Front Cell Infect Microbiol 3:73. https://doi.org/10.3389/fcimb.2013.00073.

2. Fraústo da Silva JJR, Williams RJP. 2001. The biological chemistry of the elements: the inorganic chemistry of life, 2nd ed. Oxford University Press, Oxford, United Kingdom.

3. Macomber L, Imlay JA. 2009. The iron-sulfur clusters of dehydratases are primary intracellular targets of copper toxicity. Proc Natl Acad Sci U S A 106:8344–8349. https://doi.org/10.1073/pnas.0812808106.
4. Dupont CL, Grass G, Rensing C. 2011. Copper toxicity and the origin of bacterial resistance-new insights and applications. Metallomics 3:1109–1118. https://doi.org/10.1039/c1mt00107h.
5. Osman D, Cavet JS. 2008. Copper homeostasis in bacteria. Adv Appl Microbiol 65:217–247. https://doi.org/10.1016/S0065-2164(08)00608-4.
6. Pontel LB, Soncini FC. 2009. Alternative periplasmic copper-resistance mechanisms in Gram negative bacteria. Mol Microbiol 73:212–225. https://doi.org/10.1111/j.1365-2958.2009.06763.x.
7. Espariz M, Checa SK, Audero ME, Pontel LB, Soncini FC. 2007. Dissecting the *Salmonella* response to copper. Microbiology (Reading) 153:2989–2997. https://doi.org/10.1099/mic.0.2007/006536-0.
8. González-Guerrero M, Raimunda D, Cheng X, Argüello JM. 2010. Distinct functional roles of homologous $Cu^+$ efflux ATPases in *Pseudomonas aeruginosa*. Mol Microbiol 78:1246–1258. https://doi.org/10.1111/j.1365-2958.2010.07402.x.
9. Quintana J, Novoa-Aponte L, Argüello JM. 2017. Copper homeostasis networks in the bacterium *Pseudomonas aeruginosa*. J Biol Chem 292:15691–15704. https://doi.org/10.1074/jbc.M117.804492.
10. Parmar JH, Quintana J, Ramírez D, Laubenbacher R, Argüello JM, Mendes P. 2018. An important role for periplasmic storage in *Pseudomonas aeruginosa* copper homeostasis revealed by a combined experimental and computational modeling study. Mol Microbiol 110:357–369. https://doi.org/10.1111/mmi.14086.
11. Novoa-Aponte L, Ramírez D, Argüello JM. 2019. The interplay of the metallosensor CueR with two distinct CopZ chaperones defines copper homeostasis in *Pseudomonas aeruginosa*. J Biol Chem 294:4934–4945. https://doi.org/10.1074/jbc.RA118.006316.
12. Lohmeyer E, Schroder S, Pawlik G, Trasnea PI, Peters A, Daldal F, Koch HG. 2012. The ScoI homologue SenC is a copper binding protein that interacts directly with the *cbb(3)*-type cytochrome oxidase in *Rhodobacter capsulatus*. Biochim Biophys Acta 1817:2005–2015. https://doi.org/10.1016/j.bbabio.2012.06.621.
13. Ekici S, Turkarslan S, Pawlik G, Dancis A, Baliga NS, Koch HG, Daldal F. 2014. Intracytoplasmic copper homeostasis controls cytochrome c oxidase production. mBio 5:e01055-13. https://doi.org/10.1128/mBio.01055-13.
14. Trasnea PI, Andrei A, Marckmann D, Utz M, Khalfaoui-Hassani B, Selamoglu N, Daldal F, Koch HG. 2018. A copper relay system involving two periplasmic chaperones drives cbb3-type cytochrome c oxidase biogenesis in *Rhodobacter capsulatus*. ACS Chem Biol 13:1388–1397. https://doi.org/10.1021/acschembio.8b00293.
15. Pontel LB, Scampoli NL, Porwollik S, Checa SK, McClelland M, Soncini FC. 2014. Identification of a *Salmonella* ancillary copper detoxification mechanism by a comparative analysis of the genome-wide transcriptional response to copper and zinc excess. Microbiology (Reading) 160:1659–1669. https://doi.org/10.1099/mic.0.080473-0.
16. Argüello JM, Padilla-Benavides T, Collins JM. 2013. Transport mechanism and cellular functions of bacterial $Cu^+$-ATPases, p 155–162. *In* Culotta V, Scott JA (ed), Metals in cells. Encyclopedia of inorganic and bioinorganic chemistry. Wiley & Sons, Ltd, Chichester, United Kingdom.
17. Stewart LJ, Thaqi D, Kobe B, McEwan AG, Waldron KJ, Djoko KY. 2019. Handling of nutrient copper in the bacterial envelope. Metallomics 11:50–63. https://doi.org/10.1039/c8mt00218e.
18. Neyrolles O, Wolschendorf F, Mitra A, Niederweis M. 2015. Mycobacteria, metals, and the macrophage. Immunol Rev 264:249–263. https://doi.org/10.1111/imr.12265.
19. Solioz M. 2018. Copper and bacteria: evolution, homeostasis and toxicity, p 49–80. Springer International Publishing, Cham, Switzerland.
20. Ladomersky E, Petris MJ. 2015. Copper tolerance and virulence in bacteria. Metallomics 7:957–964. https://doi.org/10.1039/c4mt00327f.
21. Hernández-Montes G, Argüello JM, Valderrama B. 2012. Evolution and diversity of periplasmic proteins involved in copper homeostasis in gamma proteobacteria. BMC Microbiol 12:249–263. https://doi.org/10.1186/1471-2180-12-249.
22. Singh K, Senadheera DB, Cvitkovitch DG. 2014. An intimate link: two-component signal transduction systems and metal transport systems in bacteria. Future Microbiol 9:1283–1293. https://doi.org/10.2217/fmb.14.87.
23. Bhagirath AY, Li Y, Patidar R, Yerex K, Ma X, Kumar A, Duan K. 2019. Two component regulatory systems and antibiotic resistance in Gram-negative pathogens. Int J Mol Sci 20:1781. https://doi.org/10.3390/ijms20071781.
24. Munson GP, Lam DL, Outten FW, O'Halloran TV. 2000. Identification of a copper-responsive two-component system on the chromosome of *Escherichia coli* K-12. J Bacteriol 182:5864–5871. https://doi.org/10.1128/jb.182.20.5864-5871.2000.
25. Gudipaty SA, Larsen AS, Rensing C, McEvoy MM. 2012. Regulation of Cu(I)/Ag(I) efflux genes in *Escherichia coli* by the sensor kinase CusS. FEMS Microbiol Lett 330:30–37. https://doi.org/10.1111/j.1574-6968.2012.02529.x.
26. Outten FW, Huffman DL, Hale JA, O'Halloran TV. 2001. The independent *cue* and *cus* systems confer copper tolerance during aerobic and anaerobic growth in *Escherichia coli*. J Biol Chem 276:30670–30677. https://doi.org/10.1074/jbc.M104122200.
27. Rouch DA, Brown NL. 1997. Copper-inducible transcriptional regulation at two promoters in the *Escherichia coli* copper resistance determinant *pco*. Microbiology 143:1191–1202. https://doi.org/10.1099/00221287-143-4-1191.
28. Grass G, Rensing C. 2001. Genes involved in copper homeostasis in *Escherichia coli*. J Bacteriol 183:2145–2147. https://doi.org/10.1128/JB.183.6.2145-2147.2001.
29. Zahid N, Zulfiqar S, Shakoori AR. 2012. Functional analysis of cus operon promoter of *Klebsiella pneumoniae* using *E. coli lacZ* assay. Gene 495:81–88. https://doi.org/10.1016/j.gene.2011.12.040.
30. Wu F, Ying Y, Yin M, Jiang Y, Wu C, Qian C, Chen Q, Shen K, Cheng C, Zhu L, Li K, Xu T, Bao Q, Lu J. 2019. Molecular characterization of a multidrug-resistant *Klebsiella pneumoniae* strain R46 Isolated from a rabbit. Int J Genomics 2019:5459190. https://doi.org/10.1155/2019/5459190.
31. Schelder S, Zaade D, Litsanov B, Bott M, Brocker M. 2011. The two-component signal transduction system CopRS of *Corynebacterium glutamicum* is required for adaptation to copper-excess stress. PLoS One 6:e22143. https://doi.org/10.1371/journal.pone.0022143.
32. Giner-Lamia J, López-Maury L, Reyes JC, Florencio FJ. 2012. The CopRS two-component system is responsible for resistance to copper in the cyanobacterium *Synechocystis sp. PCC 6803*. Plant Physiol 159:1806–1818. https://doi.org/10.1104/pp.112.200659.
33. Huertas MJ, López-Maury L, Giner-Lamia J, Sánchez-Riego AM, Florencio FJ. 2014. Metals in cyanobacteria: analysis of the copper, nickel, cobalt and arsenic homeostasis mechanisms. Life (Basel) 4:865–886. https://doi.org/10.3390/life4040865.
34. Mills SD, Jasalavich CA, Cooksey DA. 1993. A two-component regulatory system required for copper-inducible expression of the copper resistance operon of *Pseudomonas syringae*. J Bacteriol 175:1656–1664. https://doi.org/10.1128/jb.175.6.1656-1664.1993.
35. Mills SD, Lim CK, Cooksey DA. 1994. Purification and characterization of CopR, a transcriptional activator protein that binds to a conserved domain (cop box) in copper-inducible promoters of *Pseudomonas syringae*. Mol Gen Genet 244:341–351. https://doi.org/10.1007/BF00286685.
36. Zhang XX, Rainey PB. 2008. Regulation of copper homeostasis in *Pseudomonas fluorescens SBW25*. Environ Microbiol 10:3284–3294. https://doi.org/10.1111/j.1462-2920.2008.01720.x.
37. Hu YH, Wang HL, Zhang M, Sun L. 2009. Molecular analysis of the copper-responsive CopRSCD of a pathogenic *Pseudomonas fluorescens* strain. J Microbiol 47:277–286. https://doi.org/10.1007/s12275-008-0278-9.
38. Gao R, Stock AM. 2009. Biological insights from structures of two-component proteins. Annu Rev Microbiol 63:133–154. https://doi.org/10.1146/annurev.micro.091208.073214.
39. Desai SK, Kenney LJ. 2017. To ~P or not to ~P? Non-canonical activation by two-component response regulators. Mol Microbiol 103:203–213. https://doi.org/10.1111/mmi.13532.
40. Wolfe AJ. 2005. The acetate switch. Microbiol Mol Biol Rev 69:12–50. https://doi.org/10.1128/MMBR.69.1.12-50.2005.
41. Siryaporn A, Goulian M. 2008. Cross-talk suppression between the CpxA-CpxR and EnvZ-OmpR two-component systems in *E. coli*. Mol Microbiol 70:494–506. https://doi.org/10.1111/j.1365-2958.2008.06426.x.
42. Jacob-Dubuisson F, Mechaly A, Betton JM, Antoine R. 2018. Structural insights into the signalling mechanisms of two-component systems. Nat Rev Microbiol 16:585–593. https://doi.org/10.1038/s41579-018-0055-7.
43. Kenney LJ. 2010. How important is the phosphatase activity of sensor kinases? Curr Opin Microbiol 13:168–176. https://doi.org/10.1016/j.mib.2010.01.013.
44. Huffman DL, Huyett J, Outten FW, Doan PE, Finney LA, Hoffman BM, O'Halloran TV. 2002. Spectroscopy of Cu(II)-PcoC and the multicopper oxidase function of PcoA, two essential components of *Escherichia coli pco* copper resistance operon. Biochemistry 41:10046–10055. https://doi.org/10.1021/bi0259960.
45. Elsen S, Ragno M, Attree I. 2011. PtrA is a periplasmic protein involved in Cu tolerance in *Pseudomonas aeruginosa*. J Bacteriol 193:3376–3378. https://doi.org/10.1128/JB.00159-11.

46. Ha UH, Kim J, Badrane H, Jia J, Baker HV, Wu D, Jin S. 2004. An in vivo inducible gene of *Pseudomonas aeruginosa* encodes an anti-ExsA to suppress the type III secretion system. Mol Microbiol 54:307–320. https://doi.org/10.1111/j.1365-2958.2004.04282.x.
47. Affandi T, Issaian AV, McEvoy MM. 2016. The structure of the periplasmic sensor domain of the histidine kinase CusS shows unusual metal ion coordination at the dimeric interface. Biochemistry 55:5296–5306. https://doi.org/10.1021/acs.biochem.6b00707.
48. Gudipaty SA, McEvoy MM. 2014. The histidine kinase CusS senses silver ions through direct binding by its sensor domain. Biochim Biophys Acta 1844:1656–1661. https://doi.org/10.1016/j.bbapap.2014.06.001.
49. Yoneyama H, Nakae T. 1996. Protein C (OprC) of the outer membrane of *Pseudomonas aeruginosa* is a copper-regulated channel protein. Microbiology 142:2137–2144. https://doi.org/10.1099/13500872-142-8-2137.
50. Huynh TN, Stewart V. 2011. Negative control in two-component signal transduction by transmitter phosphatase activity. Mol Microbiol 82:275–286. https://doi.org/10.1111/j.1365-2958.2011.07829.x.
51. Casino P, Rubio V, Marina A. 2009. Structural insight into partner specificity and phosphoryl transfer in two-component signal transduction. Cell 139:325–336. https://doi.org/10.1016/j.cell.2009.08.032.
52. Waldron KJ, Rutherford JC, Ford D, Robinson NJ. 2009. Metalloproteins and metal sensing. Nature 460:823–830. https://doi.org/10.1038/nature08300.
53. Reyes-Caballero H, Campanello GC, Giedroc DP. 2011. Metalloregulatory proteins: metal selectivity and allosteric switching. Biophys Chem 156:103–114. https://doi.org/10.1016/j.bpc.2011.03.010.
54. Xiao Z, Brose J, Schimo S, Ackland SM, La Fontaine S, Wedd AG. 2011. Unification of the copper(I) binding affinities of the metallo-chaperones Atx1, Atox1, and related proteins: detection probes and affinity standards. J Biol Chem 286:11047–11055. https://doi.org/10.1074/jbc.M110.213074.
55. Changela A, Chen K, Xue Y, Holschen J, Outten CE, O'Halloran TV, Mondragon A. 2003. Molecular basis of metal-ion selectivity and zeptomolar sensitivity by CueR. Science 301:1383–1387. https://doi.org/10.1126/science.1085950.
56. Raimunda D, Padilla-Benavides T, Vogt S, Boutigny S, Tomkinson KN, Finney LA, Argüello JM. 2013. Periplasmic response upon disruption of transmembrane Cu(+) transport in *Pseudomonas aeruginosa*. Metallomics 5:144–151. https://doi.org/10.1039/c2mt20191g.
57. Ekici S, Yang H, Koch HG, Daldal F. 2012. Novel transporter required for biogenesis of *cbb3*-type cytochrome *c* oxidase in *Rhodobacter capsulatus*. mBio 3:e00293-11. https://doi.org/10.1128/mBio.00293-11.
58. Teitzel GM, Geddie A, De Long SK, Kirisits MJ, Whiteley M, Parsek MR. 2006. Survival and growth in the presence of elevated copper: transcriptional profiling of copper-stressed *Pseudomonas aeruginosa*. J Bacteriol 188:7242–7256. https://doi.org/10.1128/JB.00837-06.
59. Quaranta D, McCarty R, Bandarian V, Rensing C. 2007. The copper-inducible cin operon encodes an unusual methionine-rich azurin-like protein and a pre-Q0 reductase in *Pseudomonas putida KT2440*. J Bacteriol 189:5361–5371. https://doi.org/10.1128/JB.00377-07.
60. Laub MT, Goulian M. 2007. Specificity in two-component signal transduction pathways. Annu Rev Genet 41:121–145. https://doi.org/10.1146/annurev.genet.41.042007.170548.
61. Capdevila DA, Edmonds KA, Giedroc DP. 2017. Metallochaperones and metalloregulation in bacteria. Essays Biochem 61:177–200. https://doi.org/10.1042/EBC20160076.
62. Rae TD, Schmidt PJ, Pufahl RA, Culotta VC, O'Halloran TV. 1999. Undetectable intracellular free copper: the requirement of a copper chaperone for superoxide dismutase. Science 284:805–808. https://doi.org/10.1126/science.284.5415.805.
63. Arts IS, Gennaris A, Collet JF. 2015. Reducing systems protecting the bacterial cell envelope from oxidative damage. FEBS Lett 589:1559–1568. https://doi.org/10.1016/j.febslet.2015.04.057.
64. Walker KW, Gilbert HF. 1994. Effect of redox environment on the *in vitro* and *in vivo* folding of RTEM-1 beta-lactamase and *Escherichia coli* alkaline phosphatase. J Biol Chem 269:28487–28493.
65. Huston WM, Jennings MP, McEwan AG. 2002. The multicopper oxidase of *Pseudomonas aeruginosa* is a ferroxidase with a central role in iron acquisition. Mol Microbiol 45:1741–1750. https://doi.org/10.1046/j.1365-2958.2002.03132.x.
66. Singh SK, Grass G, Rensing C, Montfort WR. 2004. Cuprous oxidase activity of CueO from *Escherichia coli*. J Bacteriol 186:7815–7817. https://doi.org/10.1128/JB.186.22.7815-7817.2004.
67. Argüello JM, Patel SJ, Quintana J. 2016. Bacterial Cu(+)-ATPases: models for molecular structure-function studies. Metallomics 8:906–914. https://doi.org/10.1039/c6mt00089d.
68. Thaden JT, Lory S, Gardner TS. 2010. Quorum-sensing regulation of a copper toxicity system in *Pseudomonas aeruginosa*. J Bacteriol 192:2557–2568. https://doi.org/10.1128/JB.01528-09.
69. Outten FW, Outten CE, Hale J, O'Halloran TV. 2000. Transcriptional activation of an *Escherichia coli* copper efflux regulon by the chromosomal MerR homologue, CueR. J Biol Chem 275:31024–31029. https://doi.org/10.1074/jbc.M006508200.
70. Drees SL, Beyer DF, Lenders-Lomscher C, Lubben M. 2015. Distinct functions of serial metal-binding domains in the *Escherichia coli* P1B -ATPase CopA. Mol Microbiol 97:423–438. https://doi.org/10.1111/mmi.13038.
71. Pezza A, Pontel LB, López C, Soncini FC. 2016. Compartment and signal-specific codependence in the transcriptional control of *Salmonella* periplasmic copper homeostasis. Proc Natl Acad Sci U S A 113:11573–11578. https://doi.org/10.1073/pnas.1603192113.
72. Held K, Ramage E, Jacobs M, Gallagher L, Manoil C. 2012. Sequence-verified two-allele transposon mutant library for Pseudomonas aeruginosa PAO1. J Bacteriol 194:6387–6389. https://doi.org/10.1128/JB.01479-12.
73. Jacobs MA, Alwood A, Thaipisuttikul I, Spencer D, Haugen E, Ernst S, Will O, Kaul R, Raymond C, Levy R, Chun-Rong L, Guenthner D, Bovee D, Olson MV, Manoil C. 2003. Comprehensive transposon mutant library of *Pseudomonas aeruginosa*. Proc Natl Acad Sci U S A 100:14339–14344. https://doi.org/10.1073/pnas.2036282100.
74. Choi KH, Schweizer HP. 2006. Mini-Tn7 insertion in bacteria with single attTn7 sites: example *Pseudomonas aeruginosa*. Nat Protoc 1:153–161. https://doi.org/10.1038/nprot.2006.24.
75. Gibson DG, Smith HO, Hutchison CA, III, Venter JC, Merryman C. 2010. Chemical synthesis of the mouse mitochondrial genome. Nat Methods 7:901–903. https://doi.org/10.1038/nmeth.1515.
76. Bradford MM. 1976. A rapid and sensitive method for the quantitation of microgram quantities of protein utilizing the principle of protein-dye binding. Anal Biochem 72:248–254. https://doi.org/10.1006/abio.1976.9999.
77. Bagchi P, Morgan MT, Bacsa J, Fahrni CJ. 2013. Robust affinity standards for Cu(I) biochemistry. J Am Chem Soc 135:18549–18559. https://doi.org/10.1021/ja408827d.
78. Xiao Z, Wedd AG. 2010. The challenges of determining metal-protein affinities. Nat Prod Rep 27:768–789. https://doi.org/10.1039/b906690j.
79. Crow JP, Sampson JB, Zhuang Y, Thompson JA, Beckman JS. 1997. Decreased zinc affinity of amyotrophic lateral sclerosis-associated superoxide dismutase mutants leads to enhanced catalysis of tyrosine nitration by peroxynitrite. J Neurochem 69:1936–1944. https://doi.org/10.1046/j.1471-4159.1997.69051936.x.
80. UniProt Consortium. 2019. UniProt: a worldwide hub of protein knowledge. Nucleic Acids Res 47:D506–D515. https://doi.org/10.1093/nar/gky1049.
81. Madeira F, Park YM, Lee J, Buso N, Gur T, Madhusoodanan N, Basutkar P, Tivey ARN, Potter SC, Finn RD, Lopez R. 2019. The EMBL-EBI search and sequence analysis tools APIs in 2019. Nucleic Acids Res 47:W636–W641. https://doi.org/10.1093/nar/gkz268.
82. Waterhouse AM, Procter JB, Martin DMA, Clamp M, Barton GJ. 2009. Jalview version 2—a multiple sequence alignment editor and analysis workbench. Bioinformatics 25:1189–1191. https://doi.org/10.1093/bioinformatics/btp033.
83. Waterhouse A, Bertoni M, Bienert S, Studer G, Tauriello G, Gumienny R, Heer FT, de Beer TAP, Rempfer C, Bordoli L, Lepore R, Schwede T. 2018. SWISS-MODEL: homology modelling of protein structures and complexes. Nucleic Acids Res 46:W296–W303. https://doi.org/10.1093/nar/gky427.
84. Pettersen EF, Goddard TD, Huang CC, Couch GS, Greenblatt DM, Meng EC, Ferrin TE. 2004. UCSF Chimera–a visualization system for exploratory research and analysis. J Comput Chem 25:1605–1612. https://doi.org/10.1002/jcc.20084.